Control of Exoskeletons Inspired by Fictitious Gain in Human Model

Kyoungchul Kong, *Student Member, IEEE*, and Masayoshi Tomizuka, *Fellow, IEEE*

***Abstract*—A human wearing an exoskeleton-type assistive device results in a parallel control system that includes two controllers: an exoskeleton controller and a human brain that includes the spinal cord and the cerebrum. Unknown and complicated characteristics of the brain dynamically interact with the exoskeleton controller, which makes the controller design challenging. In this paper, the motion control system of a human is regarded as a feedback control loop that consists of the brain, muscles, and the dynamics of the extended human body. The brain is modeled as a control algorithm amplified by a fictitious gain (FG). The FG is adjusted to compensate for characteristic changes in the muscle and human body dynamics due to physical impairment, varying load, or any other causes. In this paper, an exoskeleton controller that realizes the FG is designed, and its performance and robustness are discussed.**

***Index Terms*—Assistive devices, biologically inspired control, exoskeleton.**

I. Introduction

EXOSKELETON-TYPE assistive devices have been developed for humans in battle, construction, and dangerous environments [1]–[5]. Such devices amplify the force (or torque) exerted by the human. In recent years, they are receiving an increasing attention as assistive devices for patients and the elderly in their daily lives [6]–[9]. In contrast to traditional rehabilitation devices, which are available only in limited environments such as in hospitals, the exoskeleton systems can be used anytime anywhere.

The control of exoskeletons is challenging because exoskeletons have to interact with another controller in the human body, i.e., the brain. Moreover, the performance of exoskeletons is evaluated by human feelings, so that the controllers of exoskeletons cannot be designed without considering the characteristics of the brain, which refers to the cerebrum as well as the spinal cord. If only the tracking performance is considered in the design of the exoskeleton controller, the controller may have a high gain for better rejection of disturbances, where the muscular force generated by human intention can also be considered as a disturbance from the viewpoint of the exoskeleton. In this aspect, a simple method for the control of exoskeletons is to follow the responses of the brain. For the implementation of such a method, sensing technologies for detecting the human intention play a key role. An effective sensing method is the electromyography (EMG) approach. It is known that the EMG signals are related to human joint torques and occur prior to the actual motion [10]–[12]. However, the EMG sensors have practical limitations such as the sensitivity to the sensing location and the necessity of normalization. Alternative sensing methods, such as muscle fiber expansion sensors [4] or muscle hardness sensors [13], have been developed to overcome such problems, but they do not provide a concrete solution yet.

For physically impaired persons who need assistance for rehabilitation, an impedance control method has been applied effectively [6], [9], [15]. In some applications of the impedance control, users are asked to follow predefined motions displayed on a monitor, while an assistive force is provided to compensate for the lack of muscular strength. In such cases, simple tracking controllers (e.g., a proportional–derivative (PD) controller or a lead-lag compensator) are often utilized as the impedance controller. However, this method is not appropriate to people who need assistance in their daily lives.

In this paper, a method for assisting humans is introduced; a fictitious gain (FG) is designed to increase/decrease the sensitivity of the human body. If the FG is increased, the human is assisted and able to perform demanding motions with less muscular forces. Then an exoskeleton controller is designed to realize the effects of the FG by exoskeleton systems. The concept of adjusting the sensitivity of the human body by controlling an exoskeleton was earlier proposed by Kazerooni *et al.* [3]. The exoskeleton controller designed by the FG method in this paper plays the role similar to the controller in [3], but the concept of the FG enables application of robust control theories and the intuitive design of exoskeleton controllers. Furthermore, the functions of exoskeletons can be extended from assistance to rehabilitation by selecting a proper fictitious gain.

This paper focuses mainly on the concept, the properties, and the implementation of the FG method. The effectiveness and characteristics of the proposed method are verified by simulations and experiments. In the case of assisting an elbow joint, the EMG signal is utilized as a measure of the assistance effect. For the lower extremity, a method for quantitatively evaluating the assistance effect is under development. The quantitative verification of the proposed method on the lower extremity is a topic of future publications.

II. FG in Human

A. Motion Control System in Human Body

The brain and the muscles play the roles of controller and actuator in the human body, respectively. The brain should include

Manuscript received January 26, 2009; revised July 3, 2009. First published October 20, 2009; current version published November 11, 2009. Recommended by Guest Editor V. N. Krovi. This work was supported in part by the National Science Foundation under Grant CMMI-0800501.

The authors are with the Department of Mechanical Engineering, University of California, Berkeley, CA 94720 USA (e-mail: kckong@me.berkeley.edu; tomizuka@me.berkeley.edu).

Color versions of one or more of the figures in this paper are available online at http://ieeexplore.ieee.org.

Digital Object Identifier 10.1109/TMECH.2009.2032685

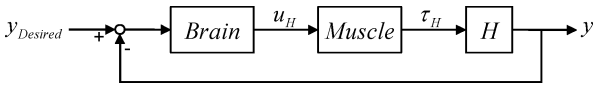

Fig. 1. Conceptual motion control structure in a human body.

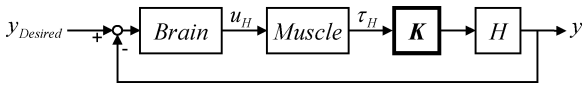

Fig. 2. Human motion control loop with an FG $\boldsymbol{K}$.

the spinal cord as well as the cerebrum [16], since reflective motions are controlled by the spinal cord and intentional motions are governed by the cerebrum.

To introduce the concept of a fictitious gain, the motion control system in a human body is regarded as a feedback control loop, as shown in Fig. 1. *Brain* in the figure refers to any organs that control human motions. H represents the musculoskeletal part of the human body, which is the system to be controlled. The brain controls muscles such that H follows the desired motion (y_{Desired}) generated by the human intention. The control output (u_H) generated by the brain is called the motor control signal or the muscle control signal, which is transferred through the motor neurons [16].

B. Concept of Fictitious Gain

In a normal motion control system in the human body shown in Fig. 1, the brain is intelligent so that it stabilizes the body robustly and adaptively. However, if the muscles are physically impaired or the load exceeds the maximum muscular force, the muscle is no longer able to execute the brain's command and requires assistance. Therefore, an FG, $K(s)$, is introduced, as shown in Fig. 2, to compensate for such physical impairment of the muscles and/or augment the muscular power.

The concept of the FG is simple; it is increased if a human needs assistance or wants to augment the muscular power. Some people, like cerebral palsy patients, suffer from tremor symptoms due to involuntary muscle contractions. In this case, the FG is decreased to reduce the power gain of the human body. When muscle spasms are severe, the FG can be designed such that the device resists motions of a certain frequency. If the gain is decreased, the exoskeleton resists human motions, and the human may feel that his/her body is heavier than before. Since the FG magnifies or reduces the power gain of the human body, it is effective for people whose motion control capability is not completely impaired.

C. Implementation of FG

The control structure of a human body interacting with an exoskeleton system is depicted in Fig. 3. By wearing the exoskeleton, the human body, H, is actuated by the sum of muscular torque, τ_H, and assistive torque, τ_A. Note that a human body wearing an exoskeleton results in a parallel control system that includes two controllers: the human brain and an exoskeleton controller.

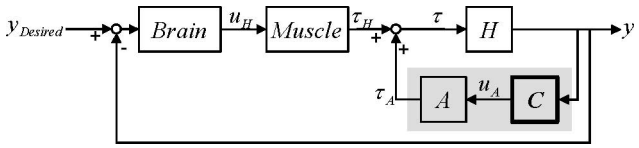

Fig. 3. Human body interacting with an exoskeleton system.

For the sake of simplicity, suppose that the motion control structure is a linear single-input–single-output (SISO) system. The following assumptions are now introduced.

1) $K(s)$ is unitarily stable, i.e., both $K(s)$ and $1/K(s)$ are stable.
2) The actuator, A in Fig. 3, is in an ideal force mode with zero impedance, i.e., $A(s) = 1$.

The first assumption makes the exoskeleton controller stable, but it imposes a constraint on the selection of the FG. By this constraint, $|K(j\omega)|$ must be nonzero for the entire frequency range.

The second assumption does not hold in actual systems because of the inertia, damping, friction, and/or any inherent nonlinearity of actuators. In this paper, such actuator dynamics is neglected (i.e., $A(s) = 1$) by assuming that a lower level control algorithm rejects the actuator dynamics effectively. The compensation of actuator dynamics for an improved physical human–robot interaction has been intensively studied in recent years. For examples, see [18] and [19]. The experimental setup in this paper will apply a rotary series elastic actuator (RSEA) that exhibits very low impedance in a force mode [19]. However, note that it is still necessary to include the mass of exoskeletons in the model of H since the extended human body dynamics has been changed by the exoskeleton. For this reason, the exoskeleton should be designed as light as possible as in [4].

The exoskeleton controller, $C(s)$ in Fig. 3, is selected such that the local feedback loop in Fig. 3 is equivalent to $H(s)$ amplified by $K(s)$, as in Fig. 2, i.e.,

$$\frac{H(s)}{1 - C(s)H(s)} = K(s)H(s). \tag{1}$$

Note that the local feedback loop in Fig. 3 has a positive feedback node. Then the exoskeleton controller is

$$C(s) = \frac{K(s) - 1}{K(s)} H^{-1}(s). \tag{2}$$

The implementation of $C(s)$ in (2) is challenged by $H^{-1}(s)$ because it is difficult to model the human body dynamics as a linear transfer function. Even if some body parts can be modeled as simple pendulums, they are not easily linearized due to the large range of human motions. Therefore, a joint torque estimate, $\hat{\tau}$, is introduced, i.e.,

$$u_A(t) = C^*(s)[\hat{\tau}(t)] \tag{3}$$

where

$$C^*(s) = \frac{K(s) - 1}{K(s)}. \tag{4}$$

Note that $\hat{\tau}$ is equal to $H^{-1}(s)[y(t)]$ in linear system cases, where $H^{-1}(s)$ is the inverse dynamics of the human body, i.e.,

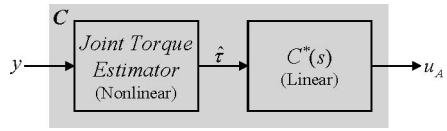

Fig. 4. Controller for exoskeleton systems realizing the fictitious gain; $C^*(s)$ is designed by (4).

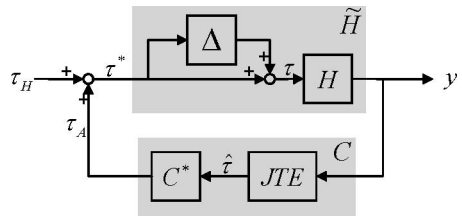

Fig. 5. Closed loop of the exoskeleton system with model uncertainties.

a transfer function from the human motion to the joint torque. If it is possible to estimate the joint torque with any appropriate methods, such as EMG sensors [11], muscle fiber expansion sensors [4], and/or muscle hardness sensors [13], $H^{-1}(s)$ is no longer required. By an appropriate joint torque estimator, an exoskeleton controller that realizes the effect of FG is designed as shown in Fig. 4; the exoskeleton controller inspired by an FG consists of $C^*(s)$ in (4) and a joint torque estimator.

Note that the controller shown in Fig. 4 determines the assistive torques by manipulating the estimated joint torques. Typical methods that simply amplify the estimated joint torques may not result in the expected performance due to the poor robustness of the overall control system. In this aspect, the advantage of the concept of FG is that it allows to design a signal processing algorithm, $C^*(s)$, considering robustness as well as performance of exoskeleton systems. Also, $C^*(s)$ can be designed to have a particular purpose, such as suppression of tremor, by intuitively selecting a proper FG. The robust stability of the proposed method will be discussed in the following section.

D. Robust Stability of Exoskeleton Controller

The estimated torque may not be accurate due to uncertainties in the measurement as well as in the parameters used in the estimation algorithm. In addition, the mechanical properties of a human body are time-varying and uncertain. Therefore, the robustness of exoskeleton controllers is critical for a safe and comfortable assistance.

Since a human body wearing an exoskeleton is actuated by the sum of human muscular torques and assistive torques, the exoskeleton takes the form of a positive feedback loop, as shown in Fig. 5 (also see the inner feedback loop in Fig. 3). Moreover, the system is governed by another controller, i.e., the brain. Therefore, the stability analysis requires to consider the brain characteristics. In the strict sense, instability in the exoskeleton loop does not necessarily mean that the overall system is unstable because the brain may be able to stabilize the unstable exoskeleton system. However, it is desired to design a stabilizing controller such that the brain does not need to perform such unnecessary tasks.

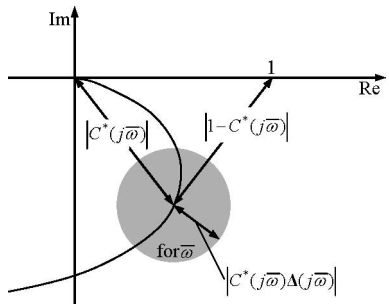

Fig. 6. Nyquist plot of L for robust stability.

Suppose that modeling uncertainties of the human body dynamics are represented by multiplicative uncertainty term Δ, as shown in Fig. 5, i.e.,

$$\tilde{H} = H(1+\Delta) \tag{5}$$

where H is the nominal human body dynamics and Δ is a random linear stable transfer function, which represents the uncertainty in the human body dynamics. The magnitude of Δ is assumed to be bounded by $|\mathbf{\Delta}|$, where $\mathbf{\Delta}$ is a fixed boundary function of the uncertainties, i.e., $|\Delta(j\omega)| \leq |\mathbf{\Delta}(j\omega)|$ for all ω.

For a simple analysis, suppose that

1) the joint torque estimator applies the inverse dynamics method (i.e., $\hat{\tau} = H^{-1}(y,t)$) and
2) the joint torque is estimated accurately (i.e., $\hat{\tau} = \tau$) and all of the uncertainties come from Δ.

The open-loop transfer function from τ^* to τ_A in Fig. 5 is

$$L = C^* H^{-1} H[1+\Delta] \tag{6}$$

where L is the open-loop transfer function. By the second assumption, the human joint torque is exactly measured or estimated such that $H^{-1}H$ is canceled. Therefore,

$$L = C^*[1+\Delta]. \tag{7}$$

Since C^* is a linear stable controller defined by (4), L is linear and stable. We now use the Nyquist stability condition to test for stability of the closed loop of the exoskeleton system, namely, the closed-loop system is stable for all L if and only if $L(j\omega)$ does not encircle the point $1 + 0j$, which is the criterion for positive feedback systems.

Fig. 6 shows the Nyquist diagram for stability analysis of L. Since Δ is unknown, it is represented as a disc, and every point on the disc is possible L. Note that $L(j\omega) = C^*(j\omega) + C^*(j\omega)\Delta(j\omega)$ from (7) and the maximum magnitude of $\Delta(j\omega)$ is $|\mathbf{\Delta}(j\omega)|$ for all ω. Therefore, the radius of the disc (i.e., the maximum amount of uncertainties) is determined by $|C^*(j\omega)\mathbf{\Delta}(j\omega)|$, as shown in Fig. 6, where $|C^*(j\bar{\omega})\mathbf{\Delta}(j\bar{\omega})|$ represents the radius of the disc at a given frequency $\bar{\omega}$. The continuous line passing through the disc is the nominal model of $L(j\omega)$, i.e., $C^*(j\omega)$. Encirclements are avoided if none of the disc intersects $(1 + 0j)$. Mathematically,

$$|C^*(j\omega)\mathbf{\Delta}(j\omega)| < |1 - C^*(j\omega)| \qquad \forall\omega. \tag{8}$$

TABLE I
CONTROL LAWS FOR CONSTANT FICTITIOUS GAINS

Gain Condition	Control Law[1)]	Effect
$k > 1$	$u_A(t) = c\hat{\tau}(t)$ [2)]	Assistance
$k = 1$	$u_A(t) = 0$	No Assistance
$0 < k < 1$	$u_A(t) = -c\hat{\tau}(t)$ [2)]	Resistance

1) Control law follows (3) and (4).
2) $c = |(k-1)/k|$.

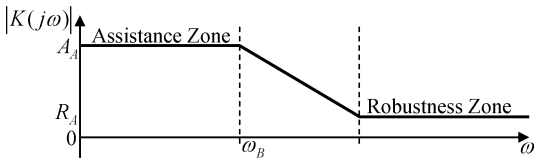

Fig. 7. Frequency-shaped FG K.

Substituting (4) into (8), a condition for the selection of the FG is

$$|K(j\omega) - 1| < |\mathbf{\Delta}(j\omega)|^{-1} \qquad \forall\omega. \tag{9}$$

Note that the condition in (9) constrains the maximum value of the FG. If the uncertainty is zero, the exoskeleton system is stable for all positive real constant FG.

E. Selection of FG

Suppose that the FG is a positive real constant gain k. In this case, the control law in (3) becomes

$$u_A(t) = \frac{k-1}{k}\hat{\tau}(t). \tag{10}$$

Depending on the magnitude of k, the control law can be divided into three states, as presented in Table I. For $k > 1$, the exoskeleton generates a torque in phase with the muscular torque. In this case, the human motion is assisted so that he/she can perform the same motion with less muscular torques. If $k = 1$, the exoskeleton does not produce any assistive torque. Similarly, for $0 < k < 1$, the torque generated by the exoskeleton is out of phase with the muscular torque and the human motion is resisted. Therefore, the control method proposed in this paper is capable of both assisting and resisting human motions according to the magnitude of the FG.

As the FG increases, the human is more assisted, but the uncertainty margin decreases by (9). Similarly, the uncertainty margin is increased as the FG decreases, but the human is less assisted or resisted. Since human motions have a certain frequency bandwidth [20], the FG can be designed as a frequency filter, as shown in Fig. 7, where the magnitude of the FG is large for better assistance in the frequency range of the human body motion and small (or close to one) for better robustness at high frequencies.

A transfer function that has the asymptotes in Fig. 7 is

$$K(s) = \frac{R_A s + A_A\omega_B}{s + \omega_B} \tag{11}$$

where A_A is an assistance factor, R_A is a robustness factor, and ω_B is the frequency bandwidth. Substituting (11) into (4), the associated exoskeleton controller $C^*(s)$ is obtained as

$$C^*(s) = \frac{(R_A - 1)s + (A_A - 1)\omega_B}{R_A s + A_A\omega_B}. \tag{12}$$

It should be noted that the uncertainty margin is infinity where the magnitude of $C^*(s)$ is 1. Fig. 8 shows the frequency responses of $K(s)$ and $C^*(s)$ with reasonable factors ($A_A = 2$, $R_A = 1$, and $\omega_B = 8$ Hz). As shown in figure, the magnitude of $K(j\omega)$ is the resulting large at low frequencies and small at high frequencies. Note that the resulting $C^*(s)$ is a low-pass filter, and thus the exoskeleton does not generate assistive forces at high frequencies that usually include large uncertainties. $C^*(s)$ in (12) will be used in simulations and experiments in Section III with various assistance factors.

Fig. 9 shows the uncertainty margins for two different types of the FG, i.e., a constant gain and a frequency-shaped filter in (11). The filter-type FG applies the same parameters as in Fig. 8. The uncertainty margins (the maximum magnitude of $\Delta(j\omega)$, i.e., $|\mathbf{\Delta}(j\omega)|$) are obtained from (9) for given FGs. At low frequencies, both FGs have the uncertainty margins of one, which means that the exoskeleton system is stable up to 100% multiplicative uncertainty at low frequencies. On the other hand, the uncertainty margin is increased at high frequencies by applying the filter-type FG (see continuous line in the figure). Note that both FGs have the same assistance factor at low frequencies, while the filter-type FG has better robustness at high frequencies.

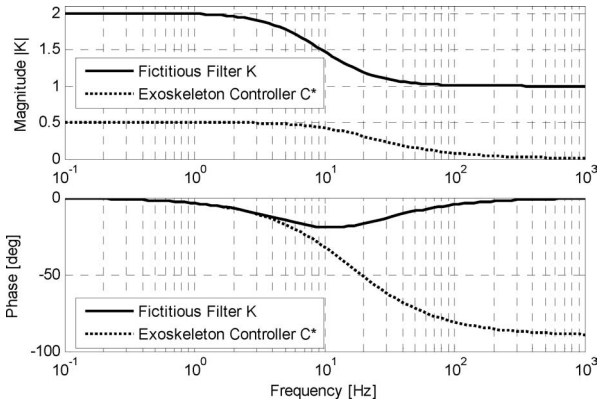

Fig. 8. Frequency responses of frequency-shaped FG and associated exoskeleton controller C^*.

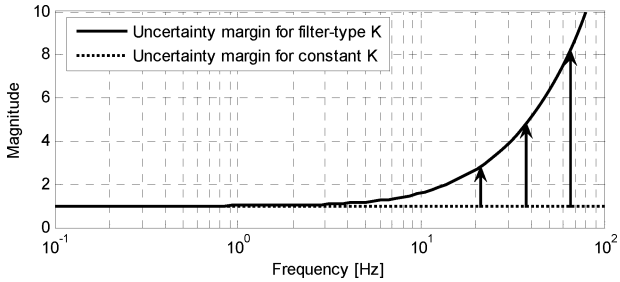

Fig. 9. Uncertainty margins for different FGs.

F. FG for Suppression of Tremor

When muscle spasms are severe so that it is desired to resist certain frequency motions as in [20], the FG can be designed as a notch filter, i.e.,

$$K(s) = \frac{s^2 + 2R_T\omega_C s + \omega_C^2}{s^2 + 2\omega_C s + \omega_C^2} \tag{13}$$

where ω_C is the center frequency and $R_T < 1$ is a factor that determines the degree of resistance. As R_T decreases, the magnitude of $K(j\omega_C)$ is decreased. The corresponding exoskeleton controller, $C^*(s)$, can be obtained from (13) based on (4).

G. FG for Multijoint Cases

For multi-input–multi-output cases (e.g., assisting the lower extremity), the human body followed by the fictitious gain, K, can be represented by HK, where K is the FG matrix and H is the multi-input–multi-output dynamics. However, the closed-loop dynamics of the human body wearing an exoskeleton is given by $[I - HC]^{-1}H$, where C is the exoskeleton controller. Suppose the human body dynamics followed by the FG is equivalent to the closed loop-dynamics, i.e.,

$$HK = [I - HC]^{-1}H. \tag{14}$$

Rearranging (14), we get

$$H[K - CHK] = H. \tag{15}$$

Note that (15) is satisfied if $K - CHK = I$, where I is an identity matrix. Therefore, the exoskeleton controller, C, is designed to satisfy (15), i.e.,

$$C = [K - I]K^{-1}H^{-1} \tag{16}$$

where H^{-1} is the inverse dynamics of the human body model. Following the same logic as in Section II-C, the exoskeleton controller can be realized by the controller, $C^*(s) = [K(s) - I]K^{-1}(s)$, and the joint torque estimator.

If the FGs are designed for each joint separately [i.e., $K_{\text{hip}}(s)$, $K_{\text{knee}}(s)$, or $K_{\text{ankle}}(s)$], K in (14)–(16) is given by diag[$K_{\text{hip}}(s)$, $K_{\text{knee}}(s)$, $K_{\text{ankle}}(s)$]. In this case, $C^*(s) = \text{diag}[\frac{K_{\text{hip}}(s)-1}{K_{\text{hip}}(s)}, \frac{K_{\text{knee}}(s)-1}{K_{\text{knee}}(s)}, \frac{K_{\text{ankle}}(s)-1}{K_{\text{ankle}}(s)}]$, and therefore, the estimated torque for each joint is processed by each controller independently. Note that the diagonal FG matrix results to decentralized exoskeleton controllers.

III. Case Study 1: Elbow Joint Assistance

The FG method proposed in this paper is verified by experiments on an elbow joint in this section.

A. System Configuration

Fig. 10 shows an assistive device called an active orthosis. The upper extremity part of the active orthosis is a single-input (τ) single-output (y) system with 1 DOF, where τ and y are the elbow joint torque and the elbow joint angle, respectively. An inclinometer provides the reference angle to an incremental encoder so that the absolute joint angle is known. The resolution of the encoder is 56 500 pulses per revolution. Due to the high resolution, it is possible to numerically calculate the first and second derivates of the encoder signal (i.e., the joint angular velocity and acceleration) in real time. Fig. 10(a) shows a simplified model of the elbow joint. The parameters m and l_C represent the mass of the forearm and the distance from the joint to the center of mass, respectively. It is assumed that m is the effective mass that includes the mass of the assistive device.

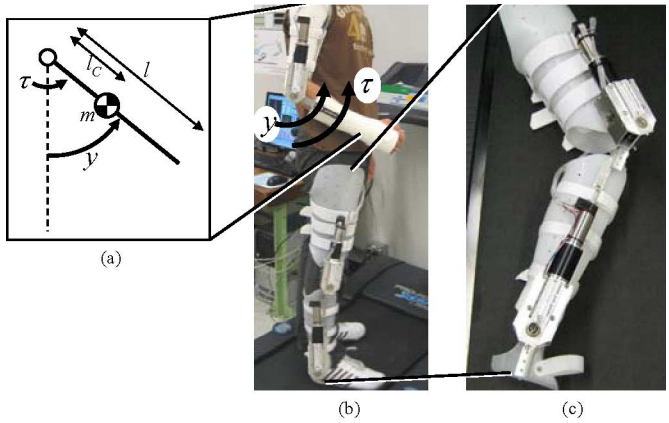

Fig. 10. Active orthosis used in experiments. (a) Simplified model for an elbow joint. (b) Active orthosis. (c) Lower extremity part.

To effectively realize the effect of the FG, an actuator is required to be in a force (torque) mode with minimum impedance. Otherwise, the actuator dynamics may affect the precision of the assistive forces and the human is not assisted as desired. The assistive device in Fig. 10 applies RSEAs [19]. The RSEA includes a torsional spring, which plays the role of an energy buffer as well as a torque sensor. The impedance compensator in [19] is applied as a lower level controller to reject the actuator dynamics such that it can be neglected in the design of an exoskeleton controller. For details on impedance compensation, see [19].

B. Joint Torque Estimator

The joint torque estimator for the elbow joint of the system shown in Fig. 10 applies the inverse dynamics method. Although the inverse dynamics is not necessarily the best option for the estimation of the joint torque, it is appropriate for this example since the physical model of the elbow joint is simple, as shown in Fig. 10(a). To obtain the physical model by the Lagrangian method, the kinetic and potential energies in the system are calculated as follows:

$$T = \frac{1}{6}ml^2\dot{y}^2 \tag{17}$$

$$V = mgl_C(1 - \cos y) \tag{18}$$

where T and V represent the kinetic energy and the potential energy, respectively. The forearm was assumed as a uniform cylinder that has mass m and length l. The equation of motion is

$$\hat{\tau} = \frac{d}{dt}\left(\frac{\partial}{\partial\dot{y}}L\right) - \frac{\partial}{\partial y}L = \frac{1}{3}ml^2\ddot{y} + mgl_C\sin y \tag{19}$$

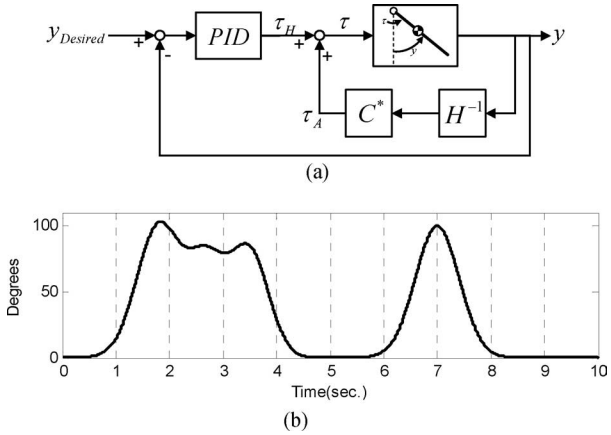

Fig. 11. Simulation setup. (a) Block diagram for simulation: C^* is obtained by the FG. (b) Desired motion in simulation.

where $L = T - V$. By using (19), the elbow joint torque can be estimated from measurements of the joint angle and the angular acceleration.

C. Simulation Study

Since the stability of exoskeletons should not be tested on human subjects due to safety issues, the elbow joint of the system in Fig. 10 was first simulated with a human body model. Also, the simulation makes it easy to verify the robustness of the proposed method to model uncertainties.

Fig. 11(a) shows a block diagram of the simulation setup. The ODE45 function in MATLAB was used to simulate the human body model. For the simulation of a human interacting with an exoskeleton system, the brain is assumed as any controller that stabilizes the body. In the block diagram in Fig. 11(a), a PID controller plays the role of the brain. The reference input, y_{Desired}, was set considering the frequency bandwidth of motions of the human elbow joint, as shown in Fig. 11(b). To verify the effectiveness of the FG, the magnitude of the muscular torque, τ_H, is observed while the elbow joint is controlled to follow the same motion.

A constant gain FG was first applied to this simulation. Four simulations were performed with different FGs (2, 1.5, 1.25, and 0.75). Fig. 12(a) shows the graphical results for $K = 2$. The simulated human in the figure successfully performed the desired motion in Fig. 11(b). Fig. 12(b) and (c) shows the simulation results for the four different gains. Note that the simulated human performed the desired motion for all of the selected FGs, while the required muscular torque has been decreased with a higher FG [see Fig. 12(c)]. In particular, note that more muscular torque was required when K is less than 1 (see $K = 0.75$ in the figure), i.e., the motion was resisted by the assistive device.

Fig. 13 shows simulation results that include model uncertainties. In the simulation, m and l were 2 kg and 0.15 m, respectively, while nominal values used in the joint torque estimator were 4 kg and 0.3 m, respectively. To compare the effect of the FG, two different types of FG were applied in the simulation: a constant gain FG ($K = 2$) and a filter-typed FG with the assistance factor of 2, which is shown in Fig. 8. Note that the

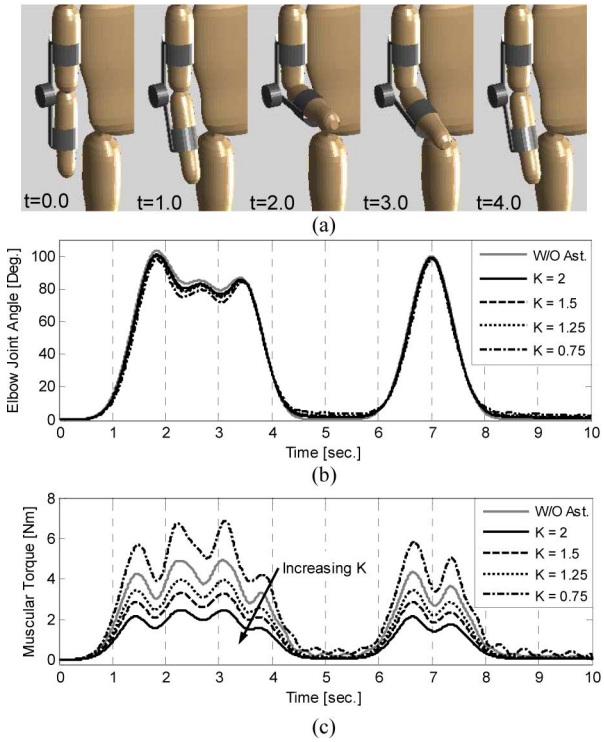

Fig. 12. Simulation results for constant FGs. (a) Simulation results for $K = 2$. (b) Performed human motions [y in Fig. 10(a)]. (c) Required human torque during the motions [τ_H in Fig. 10(a)].

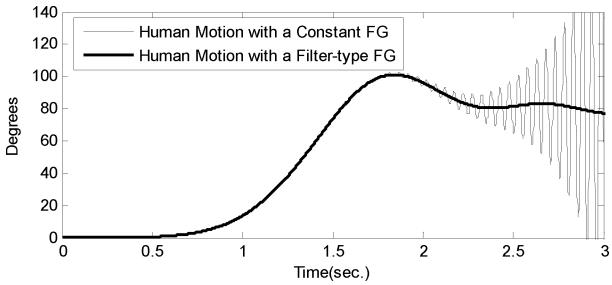

Fig. 13. Simulation results with model uncertainties.

simulation result was unstable for the constant FG and the joint angle exceeded the limit. When the filter-type FG was applied (thick line in the figure), the system was stable and performed the desired motion successfully.

D. Experimental Results

The proposed method was implemented in the system shown in Fig. 10. The FG was designed as the filter shown in Fig. 8, which was also used in the simulation. The human subject was a healthy young male whose mass and length of the forearm are 4 kg and 0.3 m approximately. Since the human determines the desired motion, only the control algorithm shown in Fig. 4 was applied without the PID controller used in the simulation. Recall that the PID controller in the simulation played the role of the human brain.

Fig. 14 shows the performed motion and the assistive torque generated by the exoskeleton controller for different assistance

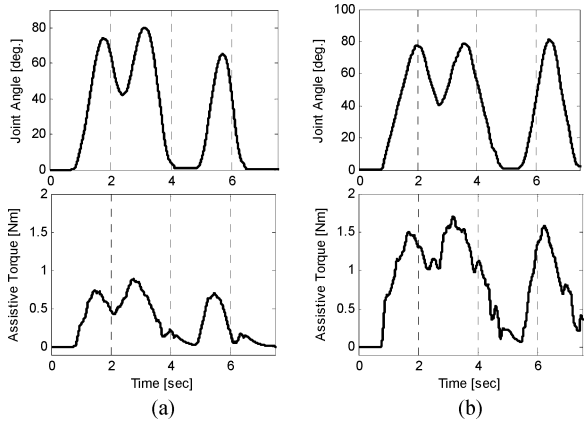

Fig. 14. Elbow joint angle and generated assistive torque during arm lifting experiments without load. (a) $K(0) = 1.5$. (b) $K(0) = 2$.

factors. The magnitude of assistive torque was increased as the gain of $K(s)$ increased, while the performed motions in Fig. 14(a) and (b) are similar, namely, the subject was more assisted with the higher gain in $K(s)$, i.e., a higher assistance factor, A_A, in (11).

The bandwidth of the FG, ω_B in (11), was set to 8 Hz in the experiments. Note that the human motion has also a limited frequency bandwidth [20], which is usually less than 8 Hz. In the experiments, the subject was not aware that the assistance factor is dependent on frequency, which implies that the device naturally assisted the human even though robustness at high frequencies is considered.

In Fig. 15, the subject is lifting a dumbbell of 3 kg. Although a heavier dumbbell could be used in the experiments, the dumbbell of 3 kg was appropriate to clearly see the effects of assistance due to the saturation of an actuator. Note that the physical model has been changed due to the mass of the dumbbell. In all the experiments, the same joint torque estimator was applied without considering the change of dynamic properties. In other words, the experiments shown in Fig. 15 verify the robustness of the proposed method. Fig. 15(b) and (c) shows the EMG signals from the biceps muscle, which is the dominant muscle that generates forces during lifting the dumbbell. The EMG signals were measured only to estimate the amount of muscular power consumed during motion, which is an indicator of assistive effect. Although it is difficult to estimate the joint torque from EMG signals accurately [11], [12], the decrease in the magnitude of EMG signal does represent the decrease of required muscular power. The EMG signals shown in the figures were filtered in real time by a moving average filter, where the width of window was 0.01 s. For a better comparison, the figures also show the postprocessed signals (see the thick continuous lines), which were filtered by a zero-phase low-pass filter (*filtfilt.m* function in MATLAB) with the cut off frequency of 1 Hz. Fig. 15(b) and (c) clearly shows that the magnitude of EMG signal was decreased significantly as the gain of $K(s)$ increased, which implies that the human was assisted effectively. The rms values of the EMG signals shown in the figures also show the effectiveness of the increased gain in $K(s)$.

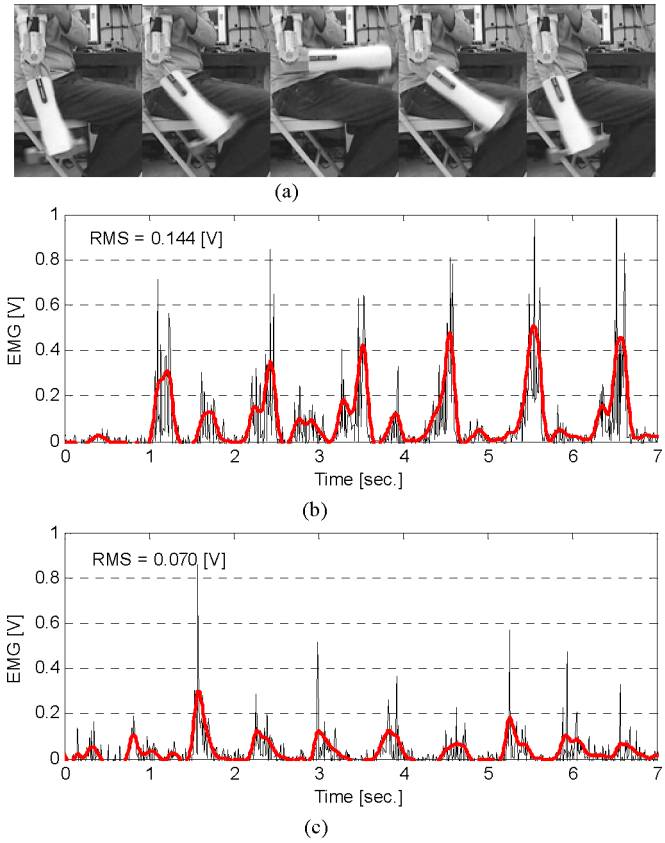

Fig. 15. Dumbbell lifting experiment; the magnitudes of EMG signals are related to the consumed muscular power. The thick continuous lines in (b) and (c) are the postprocessed signals using a zero-phase low-pass filter. (a) Snapshots of dumbbell lifting experiment. (b) EMG signal when $K(0) = 1$. (c) EMG signal when $K(0) = 2$.

IV. Case Study 2: Lower Extremity Assistance

In this section, the FG method is applied to the lower extremity. In general, assisting the lower extremity is challenging because:

1) the dynamic characteristics vary depending on the motion phases;
2) multiple joints (i.e., the hip, knee, and ankle joints) are involved; and
3) relatively larger torques are required compared to assisting the upper extremity.

Fig. 16 shows the schematic of the exoskeleton controller for assisting the lower extremity. It is assumed that three joints (i.e., the hip, knee, and ankle joints) are to be assisted. The same algorithm is applied separately for the right and left legs. The joint torque estimator may apply the inverse dynamics method, the smart shoes [14], the EMG sensors, or combinations of these methods. Note that the joint torque estimator should be properly selected according to the motion phases, because the lower extremity motions include multiple dynamics depending on the ground contact conditions. Once the joint torques are estimated, they are processed by the controller designed by the FG method [i.e., $[K(s) - I]K^{-1}(s)$ in (16)], as shown in Fig. 16.

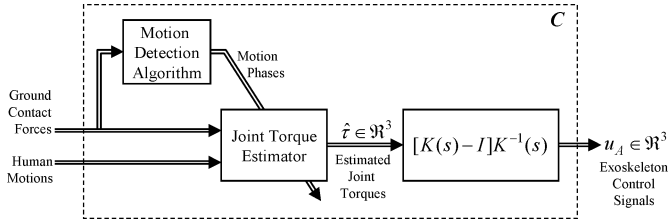

Fig. 16. Realization of fictitious gains for the lower extremity.

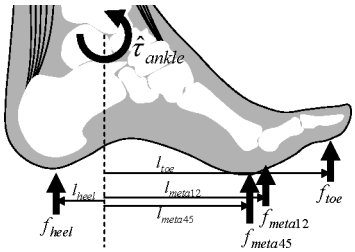

Fig. 17. Schematic of ankle joint torque estimation.

A. Estimation of Ankle Joint Torque by Smart Shoes

Smart shoes proposed by Kong and Tomizuka [14] measure forces exerted by the feet. Based on the free-body diagram of a foot, the ankle joint torques in stance phases can be calculated from the forces measured by the smart shoes. On the sagittal plane, the ankle joint torque is

$$\hat{\tau}_{\mathrm{ankle}} = f_{\mathrm{toe}} l_{\mathrm{toe}} + f_{\mathrm{meta12}} l_{\mathrm{meta12}} + f_{\mathrm{meta45}} l_{\mathrm{meta45}} - f_{\mathrm{heel}} l_{\mathrm{heel}} \tag{20}$$

where f_{toe}, f_{meta12}, f_{meta45}, and f_{heel} are the ground contact forces at the toe, the first and second metatarsophalangeal joints, and the fourth and fifth metatarsophalangeal joints, and the heel, respectively (see Fig. 17). Similarly, l_{toe}, l_{meta12}, l_{meta45}, and l_{heel} are the projected distances from the ankle joint to each ground contact point. In the experiments, the exerted forces are measured by the smart shoes, and the distances are determined by the design parameters of the smart shoes, i.e., the locations of sensors in the smart shoes. Although the estimated ankle joint torque in (20) is accurate only if the smart shoes are properly designed for each individual, utilizing the smart shoes is effective and practical in real-world systems because of the simple calculation, the low noise in the estimated torque, and the unnecessity of human body properties, which are difficult to measure (e.g., the mass of body segment).

B. Inverse Dynamics Method

In addition to (20), the inverse dynamics method can be applied to estimate the joint torques of the lower extremity. In order to use the inverse dynamics method, a human body model is necessary. Since it is necessary to integrate various algorithms (such as motion detection algorithms [14], estimation of joint torques for each motion phase [20], [21]) to use the inverse dynamics method for the lower extremity, the overall concept of the inverse dynamics method is only introduced in this paper as a part of the FG method. The detailed information on the inverse dynamics method is given in [21].

The representative models of the human body are different, depending on the ground contact conditions [20], [21], i.e., the motion phases (see Table II). The simplified models for each motion phase are also shown in Table II.

Note that the pivot point and the number of degrees of freedom of each model in Table II are different. Therefore, the joint torques calculated by different models may show discrepancy at the transition points of the motion phases. Therefore, a smoothening algorithm is necessary to avoid discomfort due to sudden changes of the assistive torques. For this purpose, a weighting vector, $\mathbf{F}$, is introduced

$$\mathbf{F} = [\,\mu_{\mathrm{IC}} \quad \mu_{\mathrm{LR}} \quad \mu_{\mathrm{MS}} \quad \mu_{\mathrm{TS}} \quad \mu_{\mathrm{PS}} \quad \mu_S\,]^T \in \Re^{6\times 1} \tag{21}$$

where μ_{IC}, μ_{LR}, μ_{MS}, μ_{TS}, μ_{PS}, and μ_S are the likelihoods of the motion phases during walking detected by the motion detection algorithm (see [14, Sec. III]). The detected likelihoods vary smoothly and continuously in [14].

Also, let $\mathbf{T_A}$ be the joint torque matrix that includes all of the joint torques calculated by all possible models, i.e.,

$$\mathbf{T_A} = [\,\hat{\tau}_{\mathrm{IC}} \quad \hat{\tau}_{\mathrm{LR}} \quad \hat{\tau}_{\mathrm{MS}} \quad \hat{\tau}_{\mathrm{TS}} \quad \hat{\tau}_{\mathrm{PS}} \quad \hat{\tau}_S\,] \in \Re^{3\times 6} \tag{22}$$

where $\hat{\tau}_{\mathrm{IC}} \in \Re^{3\times 1}$ is the calculated joint torques for the three joints in each leg (i.e., the hip, knee, and ankle joints) using the model corresponding to the initial contact phase in Table II. Similarly, $\hat{\tau}_{\mathrm{LR}}$ $\hat{\tau}_{\mathrm{MS}}$ $\hat{\tau}_{\mathrm{TS}}$ $\hat{\tau}_{\mathrm{PS}}$ and $\hat{\tau}_S$ are the joint torques calculated based on the models for the loading response, midstance, terminal stance, preswing, and swing phases, respectively.

When the leg is in the initial contact phase, the resultant joint torques should be $\hat{\tau}_{\mathrm{IC}}$, i.e., $\hat{\tau} = \mathbf{T_A}[1\ \ 0\ \ 0\ \ 0\ \ 0\ \ 0]^T$. Similarly, $[0\ \ 1\ \ 0\ \ 0\ \ 0\ \ 0]^T$ should be multiplied to $\mathbf{T_A}$ in the loading response phase. Therefore, the joint torque estimation is achieved by multiplying $\mathbf{T_A}$ in (22) and $\mathbf{F}$ in (21), i.e.,

$$\hat{\tau} = \mathbf{T_A F} \in \Re^{3\times 1}. \tag{23}$$

The sum of the components in $\mathbf{F}$ is always 1 due to a scaling factor (see [14, eq. (12)]). Also, $\mathbf{F}$ is $[1\ \ 0\ \ 0\ \ 0\ \ 0\ \ 0]^T$ if the leg is definitely in the initial contact phase, $[0\ \ 1\ \ 0\ \ 0\ \ 0\ \ 0]^T$ in the loading response, etc. Since the components in $\mathbf{F}$ (i.e., the likelihoods detected by the motion detection algorithm) vary smoothly and continuously, the resultant torque does not show sudden changes, even if $\mathbf{T_A}$ includes differently estimated joint torques. In other words, the human joint torques are estimated by interpolating the joint torques of different human body models, which correspond to each of the motion phases.

Fig. 18 shows the estimated hip, knee, and ankle joint torques during a walking experiment. The subject wore the assistive device in Fig. 10 and walked normally on a treadmill. Fig. 18(a) shows the detected motion phases during the experiment. Note that the detected phases changed smoothly, which contributed to the smooth joint torque estimation, as shown in Fig. 18(b)–(d). The joint torques are normalized with respect to the body

TABLE II
BIOMECHANICAL HUMAN BODY MODELS

Gait phases:	Initial Contact	Loading Response	Mid-Stance	Terminal Stance	Pre-Swing	Swing
Motions: [see shaded leg]	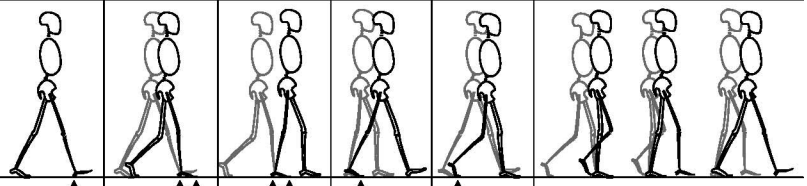					
Ground contact points:						
Representative models: ⊙: Pivot point ○: Joint ●: C. of mass	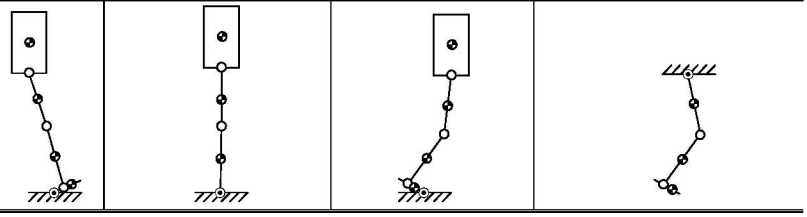					

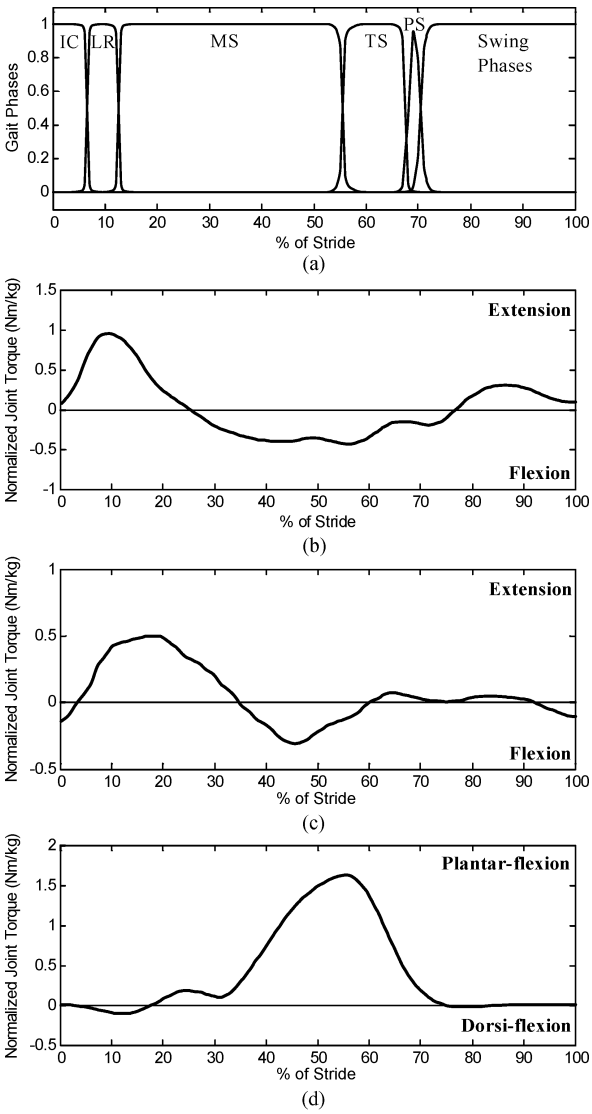

Fig. 18. Joint torque estimation based on inverse dynamics. (a) Detected gait phases. (b) Estimated hip joint torque. (c) Estimated knee joint torque. (d) Estimated ankle joint torque.

weight (note that the unit is newton meter per kilogram). In the initial contact and loading response phases (i.e., IC and LR in the figure), the hip and knee joints generated torques to the extensor direction to move the body forward. The ankle joint generated its maximum torque in the midstance and the terminal stance phases for the same reason.

V. CONCLUSION AND FUTURE WORK

In this paper, a new concept for the control of exoskeletons was proposed. The controller was designed based on an FG, which is postulated to be in the motion control system of a human body. For the analysis of the human motion control system, the brain was characterized by any fixed controller followed by the FG. The magnitude of the FG was selected according to the required amount of assistance or resistance. In addition, it was shown that the FG could be designed as a frequency-shaped filter for better robustness. Based on the designed FG, a controller for exoskeletons was obtained to implement the FG in exoskeleton systems.

The proposed method is designed by the following two major steps: 1) the design of the joint torque estimator and 2) the design of the fictitious gain. A method for designing the FG was discussed in this paper. Also, some methods were introduced for the joint torque estimator. For example, the inverse dynamics method was applied to estimate the elbow joint torque. In the case of assisting the lower extremity, various methods (motion detection algorithm proposed in [14] and inverse dynamics in [20] and [21]) were integrated.

Characteristics of the proposed method, such as performance and robustness, were discussed and verified by simulation and experiments. EMG signals were utilized as a measure of the assistance effect for the upper extremity case. For the lower extremity case, however, the characteristics and performance of the proposed method were not quantitatively analyzed in this paper, since a method for quantitatively evaluating the assistance effect is yet to be established.

ACKNOWLEDGMENT

The authors would like to thank J. Bae for supporting the experiment shown in Fig. 18.

REFERENCES

[1] E. Guizzo and H. Goldstein, "The rise of the body bots [robotic exoskeletons]," *IEEE Spectr.*, vol. 42, no. 10, pp. 50–56, Oct. 2005.
[2] (2009, Jan.). Future force warrior, International Online Defense Magazine [Online]. Available: http://www.defense-update.com/products/f/ffw-atd.htm
[3] H. Kazerooni, J. Racine, L. Huang, and R. Steger, "On the control of the Berkeley lower extremity exoskeleton (BLEEX)," in *Proc. IEEE Int. Conf. Robot. Autom.*, 2005, pp. 4353–4360.
[4] K. Kong and D. Jeon, "Design and control of an exoskeleton for the elderly and patients," *IEEE/ASME Trans. Mechatronics*, vol. 11, no. 4, pp. 428–432, Aug. 2006.
[5] HAL-5, Cyberdyne Co. (2009, Jul.). [Online]. Available: http://www.cyberdyne.jp
[6] J. Blaya and H. Herr, "Adaptive control of a variable-impedance ankle-foot orthosis to assist drop-foot fait," *IEEE Trans. Rehabil. Eng.*, vol. 12, no. 1, pp. 24–31, Mar. 2004.
[7] H. Tsukagoshi, K. Shirato, M. Ido, and A. Kitagawa, "Tail-arm: A wearable unit to stimulate exercise," in *Proc. IEEE Int. Workshop Robot Human Interactive Commun. (ROMAN)*, 2004, pp. 667–672.
[8] S. K. Banala, S. K. Agrawal, A. Fattah, V. Krishnamoorthy, W. Hsu, J. Scholz, and K. Rudolph, "Gravity-balancing leg orthosis and its performance evaluation," *IEEE Trans. Robot.*, vol. 22, no. 6, pp. 1228–1239, Dec. 2006.
[9] R. Riener, L. Lunenburger, S. Jezemik, M. Anderschitz, G. Colombo, and V. Dietz, "Patient-cooperative strategies for robot-aided treadmill training: First experimental results," *IEEE Trans. Neural Syst. Rehabil. Eng.*, vol. 13, no. 3, pp. 380–394, Sep. 2005.
[10] T. Hayashi, H. Kawamoto, and Y. Sankai, "Control method of robot suit HAL working as operator's muscle using biological and dynamical information," in *Proc. IEEE/RSJ Int. Conf. Intell. Robots Syst.*, 2005, pp. 3063–3068.
[11] O. Bida, D. Rancourt, and E. A. Clancy, "Electromyogram (EMG) amplitude estimation and joint torque model performance," in *Proc. IEEE Annu. Northeast Bioeng. Conf.*, 2005, pp. 229–230.
[12] O. F. L. Manette and M. A. Maier, "Temporal processing in primate motor control: relation between cortical and EMG activity," *IEEE Trans. Neural Netw.*, vol. 15, no. 5, pp. 1260–1267, Sep. 2004.
[13] K. Yamamoto, M. Ishii, H. Noborisaka, and K. Hyodo, "Stand alone wearable power assisting suit-sensing and control systems," in *Proc. IEEE Int. Workshop Robot Human Interactive Commun. (ROMAN)*, 2004, pp. 661–666.
[14] K. Kong and M. Tomizuka, "A gait monitoring system based on air pressure sensors embedded in a shoe," *IEEE/ASME Trans. Mechatronics*, vol. 14, no. 3, pp. 358–370, Jun. 2009.
[15] N. Hogan, "Impedance control: An approach to manipulation, Parts I, II, III," *ASME J. Dyn. Syst. Meas. Control*, vol. 107, pp. 1–23, 1985.
[16] L. Jami, *Muscle Afferents and Spinal Control of Movement*. New York: Pergamon, 1992.
[17] H. I. Krebs and N. Hogan, "Therapeutic robotics: A technology push," *Proc. IEEE*, vol. 94, no. 9, pp. 1727–1738, Sep. 2006.
[18] S. P. Buerger and N. Hogan, "Complementary stability and loop shaping for improved human-robot interaction," *IEEE Trans. Robot. Autom.*, vol. 23, no. 2, pp. 232–244, Apr. 2007.
[19] K. Kong, J. Bae, and M. Tomizuka, "Control of rotary series elastic actuator for ideal force-mode actuation in human–robot interaction applications," *IEEE/ASME Trans. Mechatronics*, vol. 14, no. 1, pp. 1–14, Feb. 2009.
[20] D. Winter, *Biomechanics and Motor Control of Human Movement*. New York: Wiley–Interscience, 1990.
[21] J. Bae, K. Kong, and M. Tomizuka, "Real-time estimation of lower extremity joint torques in normal gait," in *Proc. Int. IFAC Symp. Robot Control*, 2009, pp. 572–582.

Kyoungchul Kong (S'04) received the B.Eng. (*summa cum laude*) degree in mechanical engineering and the B.S. degree in physics, and the M.S. degree in mechanical engineering from Sogang University, Seoul, Korea, in 2004 and 2006, respectively, and the Ph.D. degree in mechanical engineering from the University of California, Berkeley, in 2009.

He is currently a Postdoctoral Researcher in the Department of Mechanical Engineering, University of California, Berkeley. He has authored or coauthored more than 40 technical articles published in various journals and conference proceedings in the area of mechatronics including human–robot interaction and assistive systems. His research interests include design, modeling, and control of mechatronic systems with emphasis on betterment of quality of human life.

Dr. Kong was the recipient of the Best Student Paper Award at the IEEE Conference on Advanced Intelligent Mechatronics in 2008, the Best Paper Award in the Division of Dynamic Systems and Control at the Korean Society of Mechanical Engineers Annual Conference in 2005, and the Best Poster Award at the Third Center of Intelligent Robot Workshop in 2005.

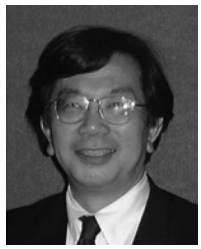

Masayoshi Tomizuka (M'86–SM'95–F'97) was born in Tokyo, Japan, in 1946. He received the B.S. and M.S. degrees from Keio University, Tokyo, in 1968 and 1970, respectively, and the Ph.D. degree from Massachusetts Institute of Technology, Cambridge, all in mechanical engineering.

In 1974, he joined the Department of Mechanical Engineering, University of California, Berkeley, where he is currently the Cheryl and John Neerhout, Jr., Distinguished Professor Chair. His research interests include optimal and adaptive control, digital control, signal processing, motion control, and control problems related to robotics, machining, manufacturing, and information storage devices and vehicles. He was the Technical Editor of the *ASME Journal of Dynamic Systems, Measurement and Control (J-DSMC)* (1988–1993). He has also been an Associate Editor of the *Journal of the International Federation of Automatic, Control, Automatica*, and the *European Journal of Control*.

Prof. Tomizuka is a Fellow of the American Society of Mechanical Engineers (ASME) and the Society of Manufacturing Engineers. He was the Editor-in-Chief of the IEEE/ASME TRANSACTIONS ON MECHATRONICS from 1997 to 1999. He was the General Chairman of the 1995 American Control Conference and the President of the American Automatic Control Council during 1998–1999. He was the recipient of the J-DSMC Best Paper Award (1995), the DSCD Outstanding Investigator Award (1996), the Charles Russ Richards Memorial Award (ASME, 1997), the Rufus Oldenburger Medal (ASME, 2002), and the John R. Ragazzini Award (2006).